Energy transfer in CaF_2 doped with Ce^{3+}, Eu^{2+} and Mn^{2+} ions

Energy transfer in CaF_2 doped with Ce^{3+}, Eu^{2+} and Mn^{2+} ions

U Caldiño G

Departamento de Física, Universidad Autónoma Metropolitana-Iztapalapa, PO Box 55-534, 09340 México, DF, Mexico

E-mail: cald@xanum.uam.mx

Abstract
The optical properties of calcium fluoride triply doped with cerium, europium and manganese ions have been analyzed in the present investigation. The spectroscopic data obtained clearly indicate that energy transfer takes place from tetragonal Ce^{3+}–F_{int}^{-} ions to Eu^{2+} and Mn^{2+} ions. Such energy transfer occurs via a short-range interaction mechanism into Ce^{3+}–Eu^{2+} and Ce^{3+}–Mn^{2+} clusters formed in the crystalline matrix. In contrast to the $Eu^{2+} \rightarrow Mn^{2+}$ energy transfer usually observed in CaF_2:Eu^{2+}:Mn^{2+}, manganese ions do not appear to be sensitized by europium ions, which might suggest that Eu^{2+} ions prefer to cluster with tetragonal Ce^{3+} ions when these ions are also present in the lattice. This preferential impurity clustering appears to be a quite relevant finding for the design of more efficient laser systems or conversion phosphors of ultraviolet to visible light. The number of tetragonal cerium ions associated with activator ions (europium or manganese) was estimated using a simple model describing the essential features of the kinetics of the $Ce^{3+} \rightarrow Eu^{2+}$ and $Ce^{3+} \rightarrow Mn^{2+}$ energy transfers.

1. Introduction

The phenomenon of resonant energy transfer among impurity ions in a solid material has been the subject of a considerable amount of work during recent decades. The interest in this field arises because energy transfer is important in the development of fibre-optic amplifiers used in communication devices [1–4], efficient phosphor materials (such as radiation detectors [5] and flat panel displays [6]) and solid state laser systems, in which the energy processes can cause an enhancement of the luminescence emission resulting in a reduction of the laser threshold [7, 8].

The processes of non-radiative energy transfer between different optically active ions have been examined in several host materials. From such materials calcium fluoride is a compound of single structure with high solubility of both sensitizer and activator ions, which permits

the preparation of efficient phosphor samples over a wide range of concentrations. Trivalent (Re^{3+}) or divalent (Re^{2+}) rare-earth ions enter the CaF_2 lattice substitutionally for Ca^{2+} ions, residing in a variety of sites. Re^{2+} ions or non-locally compensated Re^{3+} ions form centres of octahedral cubic symmetry. The Re^{3+} ion can also be charge compensated by F^- interstitials in either nearest-neighbour or next-nearest-neighbour positions, forming tetragonal (C_{4v}) or trigonal (C_{3v}) centres, respectively. Clustering of such defects readily occurs, resulting in a variety of possible cluster configurations. However, in CaF_2 the C_{4v} centres appear to be dominant for all rare earths [9]. From the Re^{3+} ions the Ce^{3+} ion has been used as a sensitizer in energy transfer processes taking place in CaF_2 crystals, due to its versatile spectroscopic properties. For example, an efficient pumping of Mn^{2+} ions in such a crystal can be achieved using Ce^{3+} ions as sensitizers [10, 11]. This energy transfer process takes place predominantly from Ce^{3+} ions locally charge compensated by F^- interstitials in nearest-neighbour positions (in $\langle 110 \rangle$ directions) forming tetragonal centres (Ce^{3+}–F_{int}^- centres) [11]. Moreover, such a transfer occurs into small Ce^{3+}–Mn^{2+} clusters formed in the lattice [12]. From the Re^{2+} ions the Eu^{2+} ion has also shown to be an excellent sensitizer of Mn^{2+} ions in CaF_2 due to its intense and broad absorption bands and its strong tendency to cluster with Mn^{2+} ions [13]. Mn^{2+} and Eu^{2+} ions enter substitutionally for Ca^{2+}, which has an eightfold coordination environment. Eu^{2+} ions have also been used as activators of tetragonal Ce^{3+} ions in CaF_2, in which the transfer occurs into small Ce^{3+}–Eu^{2+} clusters formed in the crystal [14].

The optical properties of CaF_2 doped with Mn^{2+}, Ce^{3+} or Eu^{2+} ions have previously been analysed by several workers [15–19]. Mn^{2+} ions in CaF_2 have played an important role as activators of this important phosphor material, widely used as a thermoluminescent dosimeter. Considering that the d $\rightarrow$ d absorption transitions of Mn^{2+} ions are difficult to pump, since they are forbidden by spin and parity for electric dipole radiation in octahedral complexes, their absorption (excitation) bands in CaF_2 have been studied from the excitation spectrum of the Mn^{2+} emission. Such bands have been attributed to transitions from the ground state $^6A_{1g}(S)$ to different excited levels in a cubic environment [16, 17]. Excitation within any of such bands induces the emission characteristic of Mn^{2+} ions peaking at $\sim$490 nm, with a lifetime value of $\sim$87 ms [13], which is associated with the transition from the $^4T_{1g}(G)$ lower excited level to the $^6A_{1g}(S)$ ground state.

The absorption spectrum at low concentration of Ce^{3+} ions in CaF_2 mainly consists of two bands, labelled A (peaking at $\sim$305 nm) and B (peaking at $\sim$200 nm) in increasing order of energy. Loh [18] attributed such bands to the absorption 4f $\rightarrow$ 5d of tetragonal Ce^{3+}–F_{int}^- ions. As the cerium concentration increases, two additional bands, called C (peaking at $\sim$240 nm) and D (peaking at $\sim$218 nm), appear in the absorption spectrum. These two bands have been associated with the transitions 4f $\rightarrow$ 5d of tetragonal Ce^{3+}–F_{int}^- ions forming aggregates of an unknown structure. Excitation within either the A or B absorption bands induces the emission characteristic of Ce^{3+} ions in tetragonal sites, with a lifetime value of $\sim$1 μs [12, 20]. Such an emission consists of two bands peaking at $\sim$320 and 340 nm. These bands are associated with transitions from the $^2D_{3/2}$ excited level to the ground state, which is split into its $^2F_{5/2}$ and $^2F_{7/2}$ components by spin–orbit interaction [14]. The absorption spectrum of Eu^{2+} ions in CaF_2 consists of two broad bands in the ultraviolet (UV) region, which are attributed to the electric dipole allowed $4f^7(^8S_{7/2}) \rightarrow 4f^65d(T_{2g})$ and $4f^7(^8S_{7/2}) \rightarrow 4f^65d(E_g)$ transitions [19]. Excitation with light lying in either of such bands produces only one broad emission band peaking at $\sim$424 nm with a lifetime value of $\sim$0.7 μs [13], which is associated with the transition from the $4f^65d(E_g)$ excited level to the $4f^7(^8S_{7/2})$ ground state.

Taking into account that energy transfers $Ce^{3+} \rightarrow Mn^{2+}$, $Eu^{2+} \rightarrow Mn^{2+}$ and $Ce^{3+} \rightarrow Eu^{2+}$ have previously been observed and studied in CaF_2:Ce^{3+}:Mn^{2+} [10–12], CaF_2:Eu^{2+}:Mn^{2+} [13] and CaF_2:Ce^{3+}:Eu^{2+} [14], the optical properties of calcium fluoride containing Ce^{3+}, Eu^{2+}

and Mn^{2+} ions have been analysed from photoluminescence measurements in the present investigation.

2. Experimental details

The single crystal of CaF$_2$:Ce^{3+}:Eu^{2+}:Mn^{2+} studied in this work was grown by Optovac Inc. using a double crucible technique to minimize oxygen contamination. In fact, the absorption and luminescence spectra did not exhibit any features which could be attributed to the presence of oxygen. The standard mechanical polishing technique utilizing alumina polishing abrasives was used to prepare crystal surfaces for optical absorption and photoluminescence measurements. Cerium concentration was determined from their A-absorption band using Smakula's equation with a value for the oscillator strength of 4.8×10^{-3} [11]. The concentration resulted in being $\sim 2.2 \times 10^{18}$ cm^{-3} ($\sim$160 ppm), which is lower than that added to the melt, and hence, the remaining Ce^{3+} ions can be accounted for by Ce^{3+} aggregates associated with the C and D absorption bands. Such an estimation was achieved using a Perkin-Elmer λ-5 double beam recording spectrophotometer. The manganese ion concentration ($\sim 1.2 \times 10^{20}$ cm^{-3} or $\sim$3446 ppm) was estimated by atomic absorption spectrophotometry. Divalent europium was found in the crystal as an unintentional impurity. Its concentration was estimated to be lower than 1 ppm ($\sim 1 \times 10^{15}$ cm^{-3}) as revealed from optical absorption spectrum of the crystal.

Continuous emission and excitation spectra were obtained with a Perkin-Elmer 650-10S spectrofluorimeter equipped with a 150 W xenon lamp and a red sensitive Hamamatsu R928 photomultiplier tube. Lifetime data of the manganese emission were carried out by using a Perkin-Elmer model LS-5 spectrofluorimeter, equipped with a 20 W pulsed xenon lamp, which was operated in the phosphorescence mode.

Low-temperature measurements were carried out with an Air Products DE-202 He-closed-cycle cryostat refrigerator.

3. Results

Figure 1 portrays the room-temperature (RT) emission spectrum of a CaF$_2$ crystal containing Ce^{3+}, Eu^{2+} and Mn^{2+} ions when excitation is performed with 306 nm light lying within the A-absorption band of tetragonal Ce^{3+}–F$_{int}^{-}$ ions. The spectrum consists of two UV bands, peaking at $\sim$320 and 342 nm, a blue band, peaking at $\sim$424 nm, and a green band, peaking at $\sim$502 nm. The UV bands correspond to the de-excitation of tetragonal Ce^{3+}–F$_{int}^{-}$ ions from the excited state ^{2}D$_{3/2}$ to the ^{2}F$_{5/2}$ and ^{2}F$_{7/2}$ components of the ground state. The blue emission has the same characteristics as the Eu^{2+} emission band observed in CaF$_2$:Eu^{2+} [13, 19], and therefore it can be attributed to the 4f^{6}5d(E$_g$) $\rightarrow$ 4f^7(^{8}S$_{7/2}$) transition of Eu^{2+} ions. The green band was found to shift to longer wavelengths when the sample temperature was lowered. This behaviour is usually observed for the Mn^{2+} emission [13]. The green band was, therefore, attributed to the ^{4}T$_{1g}$(G) $\rightarrow$ ^{6}A$_{1g}$(S) transition of Mn^{2+} ions.

Excitation at 245 nm, which lies within the Eu^{2+} ion 4f^{6}5d(T$_{2g}$) and tetragonal Ce^{3+}–F$_{int}^{-}$ ion C-absorption bands, produces two additional UV bands peaking at about 293 and 380 nm, associated with emissions of tetragonal Ce^{3+} aggregates. However, the Eu^{2+} ion blue emission is not observed, since it is hidden by the intense and broad band of 380 nm emission.

The inset in figure 1 displays the emission spectrum obtained under excitation at 340 nm, which lies within the Eu^{2+} ion 4f^7(^{8}S$_{7/2}$) $\rightarrow$ 4f^{6}5d(E$_g$) and Mn^{2+} ion ^{6}A$_{1g}$(S) $\rightarrow$ ^{4}T$_{2g}$(D) absorption transitions. The spectrum consists of the typical emissions of europium and
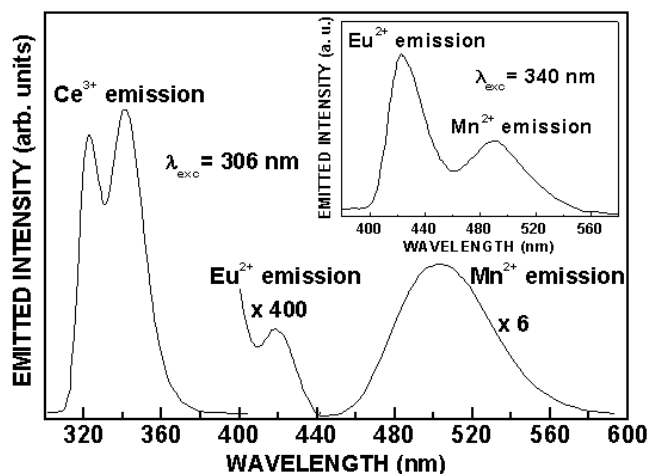
Figure 1. RT emission spectrum under excitation within the Ce^{3+} A-absorption band at 306 nm. The inset shows the emission spectrum under excitation at 340 nm.

manganese in CaF$_2$, which peak at $\sim$424 and 490 nm, respectively. It can be noted that the tetragonal Ce^{3+}-sensitized Mn^{2+} emission peaks at longer wavelength ($\sim$502 nm) than the manganese emission induced by 340 nm excitation. Such a longer wavelength of the tetragonal Ce^{3+}-sensitized Mn^{2+} emission has been explained on the basis of a larger crystal field splitting around the Mn^{2+} ions coupled with tetragonal Ce^{3+}–F$_{int}^{-}$ ions [11].

The RT excitation spectra of the europium and manganese emissions, monitored at $\lambda_{em} = 430$ and 500 nm, respectively, are portrayed in figure 2. The excitation spectrum of the emission of Eu^{2+} ions not only contains their 4f^7(^{8}S$_{7/2}$) $\rightarrow$ 4f^{6}5d(E$_g$) absorption transition but also the A-absorption band of tetragonal Ce^{3+} ions (figure 2(a)). In the same way, the excitation spectrum of the emission of Mn^{2+} ions also contains such an absorption band of Ce^{3+} ions in addition to their ^{6}A$_{1g}$(S) $\rightarrow$ ^{4}T$_{1g}$(G), ^{6}A$_{1g}$(S) $\rightarrow$ ^{4}T$_{2g}$(G), ^{6}A$_{1g}$(S) $\rightarrow$ ^{4}A$_{1g}$, ^{4}E$_g$(G) and ^{6}A$_{1g}$(S) $\rightarrow$ ^{4}T$_{2g}$(D) absorption transitions (figure 2(b)). The C-absorption band due to tetragonal Ce^{3+} aggregates is clearly observed in the excitation spectrum of the Mn^{2+} emission (figure 2(b)), whereas such an absorption band cannot be resolved in the excitation spectrum of the Eu^{2+} emission (figure 2(a)), because of its overlap with the 4f^7(^{8}S$_{7/2}$) $\rightarrow$ 4f^{6}5d(T$_{2g}$) absorption band of Eu^{2+} ions in the same wavelength region.

The manganese luminescence decay was found to consist of a single exponential decay, whose lifetime ($\sim$80 ms at RT) increases at low temperature ($\sim$160 ms at 20 K). This decay scheme was found to be similar to that determined in a powder sample of CaF$_2$:Mn^{2+} ($\sim$5000 ppm) [13]. Such an increase in the lifetime of the Mn^{2+} ions can be explained considering that the probabilities of the phonon-assisted and non-radiative processes are quite reduced at low temperature [21].

4. Discussion

The presence of the A-absorption band of tetragonal Ce^{3+} ions in the excitation spectra of the Eu^{2+} and Mn^{2+} emissions provides clear evidence that Ce^{3+} $\rightarrow$ Eu^{2+} and Ce^{3+} $\rightarrow$ Mn^{2+} energy transfers take place in the triply doped crystal. In fact, the Eu^{2+} and Mn^{2+} emissions observed under A-band excitation of tetragonal Ce^{3+}–F$_{int}^{-}$ ions (at 306 nm) are due to such energy transfer processes, since the Eu^{2+} and Mn^{2+} ions cannot be directly excited into 306 nm
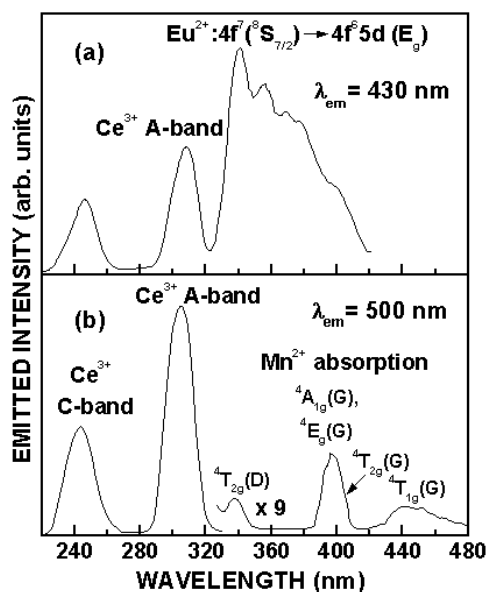
Figure 2. RT excitation spectra of (a) the Eu^{2+} emission taken at 430 nm and (b) the Mn^{2+} emission taken at 500 nm.

wavelength. Moreover, these processes are expected to occur considering that the cerium emission produced by A-band excitation overlaps the europium $4f^7(^8S_{7/2}) \rightarrow 4f^65d(E_g)$ and manganese $^6A_{1g}(S) \rightarrow ^4T_{2g}(D)$ and $^6A_{1g}(S) \rightarrow ^4E_g(D)$ absorptions, as can be appreciated from the spectra shown in figure 3. This figure also shows the emission spectrum of cerium aggregates (dashed curve), in which it can be appreciated that such an emission (obtained with 245 nm excitation) also overlaps with the same Eu^{2+} and Mn^{2+} ion absorptions. Therefore, the tetragonal Ce^{3+}–F$^-_{int}$ ion aggregates could also take part in energy transfer to Eu^{2+} and Mn^{2+} ions. Considering that the C-absorption band due to tetragonal cerium aggregates is clearly observed in the excitation spectrum of the Mn^{2+} emission (figure 2(b)), it can be inferred that such aggregates take part in energy transfer to Mn^{2+} ions.

Taking into account that the excitation spectrum of the Mn^{2+} emission (figure 2(b)) does not contain the Eu^{2+} ion $4f^7(^8S_{7/2}) \rightarrow 4f^65d(E_g)$ absorption band observed in the spectrum of figure 2(a), it can, then, be inferred that Mn^{2+} ions do not become sensitized by Eu^{2+} ions, in spite of the fact that the Eu^{2+} emission overlaps with the $^6A_{1g}(S) \rightarrow ^4T_{1g}(G)$ Mn^{2+} ion absorption in CaF$_2$ [13]. In fact, it was not possible to observe, even at very high resolution conditions of the spectrofluorimeter, the green emission of Mn^{2+} ions under 360 nm excitation (lying within the Eu^{2+} ion $4f^7(^8S_{7/2}) \rightarrow 4f^65d(E_g)$ absorption band), in which direct excitation of Mn^{2+} ions cannot be achieved. This is in contrast to the active energy transfer from Eu^{2+} to Mn^{2+} ions observed in CaF$_2$ doubly doped with these ions, which takes place into Eu^{2+}–Mn^{2+} clusters formed in the lattice [13]. These experimental observations suggest that Eu^{2+} ions do not interact with Mn^{2+} ions, and therefore it can be assumed that two different cluster types, Ce^{3+}–Eu^{2+} and Ce^{3+}–Mn^{2+}, are participating in the energy transfer from tetragonal Ce^{3+}–F$^-_{int}$ ions to Eu^{2+} and Mn^{2+} ions in the triply doped crystal.

Although it is not possible to unambiguously identify the nature of the Ce^{3+}–Eu^{2+} and Ce^{3+}–Mn^{2+} interactions producing the energy transfer from tetragonal cerium ions to europium and manganese ions, it is expected that a short-range interaction mechanism is active between
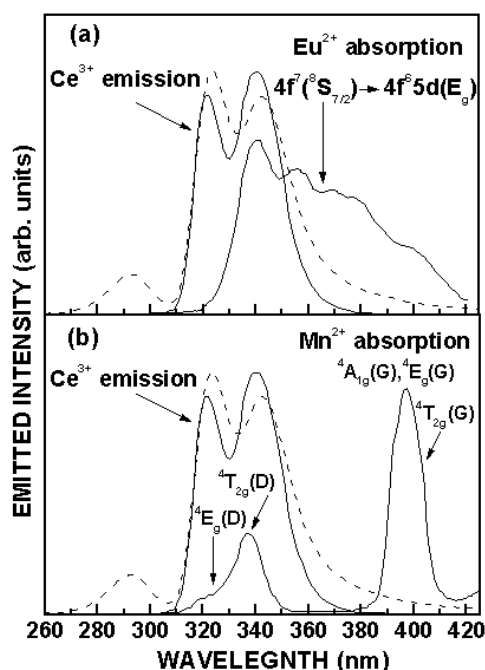
Figure 3. RT overlap region of the tetragonal cerium emission and (a) europium absorption and (b) manganese absorption. The cerium aggregate emission is shown by the dashed curve.

such ions. Considering that the absorption transitions of the tetragonal Ce^{3+} and Eu^{2+} ions are electric dipole allowed, it is expected that the energy transfer mechanism between such ions is of the electric dipole–dipole type [14, 22, 23]. On the other hand, the long lifetime measured for the manganese emission reveals the forbidden nature of the 3d $\rightarrow$ 3d transitions, and therefore it is expected that the energy transfer mechanism between tetragonal Ce^{3+} and Mn^{2+} ions is of the electric dipole–quadrupole type [12].

The transfer rate $W_{\mathrm{DD}}^{\mathrm{sa}}$ for the electric dipole–dipole interaction between tetragonal Ce^{3+} and Eu^{2+} ions (assuming that the field strength in the medium is equal to that in air) is given by [24]:

$$W_{\mathrm{sa}}^{\mathrm{DD}} = \frac{3\hbar^4 c^4}{4\pi n^4 \tau_{\mathrm{s}}^{\mathrm{o}}} \left(\frac{1}{R_{\mathrm{sa}}}\right)^6 Q_{\mathrm{a}}\Omega, \tag{1}$$

where $\Omega = \int [F_{\mathrm{s}}(E)F_{\mathrm{a}}(E)/E^4]\,\mathrm{d}E$ represents the spectral overlap integral between the normalised shapes of the tetragonal Ce^{3+} ion emission $F_{\mathrm{s}}(E)$ and Eu^{2+} ion absorption $F_{\mathrm{a}}(E)$, E being the transfer energy, Q_{a} is the integrated absorption coefficient of the europium ions, R_{sa} is the interaction distance between the tetragonal Ce^{3+} and Eu^{2+} ions involved in the transfer and $\tau_{\mathrm{s}}^{\mathrm{o}}$ is the Ce^{3+} ion intrinsic lifetime in the absence of energy transfer. The other symbols in equation (1) have their usual meaning. Because the optical absorption spectrum of the Eu^{2+} ions was hardly detectable due to their very low concentration, even at very high resolution conditions of the optical spectrophotometer, the integrated absorbance of the Eu^{2+} ions was estimated from the relationship given by Blasse [25]:

$$Q_{\mathrm{a}} = 4.8 \times 10^{-20} \ \mathrm{eV} \ \mathrm{m}^2 \cdot f_{\mathrm{d}}, \tag{2}$$

where the electric dipole oscillator strength, f_{d}, is about 0.02 for Eu^{2+} ions. The overlap integral was calculated using the normalised line-shape functions for the cerium emission (obtained
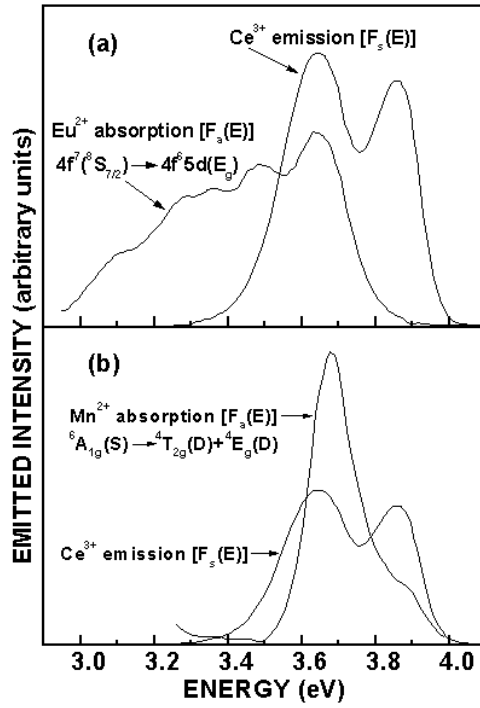
Figure 4. RT overlap region between the normalised line-shape functions of the Ce^{3+}–F$^-_{\text{int}}$ emission and (a) Eu^{2+} absorption, (b) Mn^{2+} absorption.

under A-absorption band excitation) and europium absorption at RT in the overlap region, which are portrayed in figure 4(a). The value of Ω was found to be 6.2×10^{-3} eV^{-5}. Using these values for Q_a and Ω, the critical interaction distance (defined as the distance at which the energy transfer rate is equal to the intrinsic rate of the sensitizer ions, i.e., $W^{\text{DD}}_{\text{sa}} \tau^o_s = 1$) was estimated from equation (1). The result was $\sim$26 Å.

The transfer rate $W^{\text{DQ}}_{\text{sa}}$ for the electric dipole–quadrupole interaction between tetragonal Ce^{3+} and Mn^{2+} ions can be determined from the following relation [24]:

$$W^{\text{DQ}}_{\text{sa}} = \frac{3\hbar^4 c^4 f_q \lambda^2_s}{4\pi n^4 \tau^o_s f_d} \left(\frac{1}{R_{\text{sa}}}\right)^8 Q_a \Omega, \tag{3}$$

where λ_s is the wavelength position of the cerium emission, and f_q ($\sim$10^{-10}) and f_d ($\sim$10^{-7}) are the oscillator strengths of the Mn^{2+} ion electric quadrupole and dipole transitions, respectively. Because the small absorption coefficient of manganese is difficult to measure, Q_a ($\approx$4.8 $\times$ 10^{-27} eV m^2) was estimated using relationship (2). The overlap integral Ω was estimated from the normalised line-shape functions for the cerium emission $F_s(E)$ (induced by A-absorption band excitation) and manganese absorption $F_a(E)$ at RT in the overlap region, which are displayed in figure 4(b). To obtain $F_a(E)$ we employed the excitation spectrum of Mn^{2+} in CaF$_2$ reported by Alonso and Alcalá [21]. The value of Ω was found to be 1.2×10^{-2} eV^{-5}. Using these values for Q_a and Ω, the critical interaction distance (distance at which $W^{\text{DQ}}_{\text{sa}} \tau^o_s = 1$) was estimated from equation (3). The result was $\sim$9 Å.

As expected, the critical interaction distance between tetragonal Ce^{3+}–F$^-_{\text{int}}$ and Eu^{2+} ions has resulted in being long as compared to that between tetragonal Ce^{3+}–F$^-_{\text{int}}$ and Mn^{2+} ions,

Table 1. Calculated rates using an electric dipole–dipole mechanism (W_{Ce-Eu}^{DD}) for the $Ce^{3+} \rightarrow Eu^{2+}$ energy transfer and an electric dipole–quadrupole mechanism (W_{Ce-Mn}^{DQ}) for the $Ce^{3+} \rightarrow Mn^{2+}$ energy transfer between sensitizer–activator ions at first (D_1 complex), second (D_2 complex) and third (D_3 complex) neighbours.

| Complexes | Interaction | Energy transfer rate (s^{-1}) | |
Ce–Eu and Ce–Mn	distance (Å)	W_{Ce-Eu}^{DD}	W_{Ce-Mn}^{DQ}
D_1	3.86	1.6×10^{11}	1.1×10^9
D_2	5.45	2.0×10^{10}	6.9×10^7
D_3	6.68	5.8×10^9	1.4×10^7

since it is well known that an electric dipole–dipole interaction mechanism induces a higher probability of energy transfer than an electric quadrupole–dipole one.

The rates of $Ce^{3+} \rightarrow Eu^{2+}$ energy transfer via an electric dipole–dipole interaction mechanism and those corresponding to $Ce^{3+} \rightarrow Mn^{2+}$ energy transfer via an electric dipole–quadrupole interaction mechanism at first, second and third neighbours (complexes D_1, D_2 and D_3 portrayed in figure 5 of [12]) were estimated from equations (1) and (3), respectively, using the fluorescence decay datum previously reported [12, 20] for the cerium emission. The results obtained are given in table 1, in which it can be appreciated that such rates are quite high as compared to the intrinsic radiative decay rate of the tetragonal Ce^{3+} sensitizer ions ($\sim 1 \times 10^6$ s^{-1}). From the table it can also be appreciated that the rate of $Ce^{3+} \rightarrow Eu^{2+}$ energy transfer is much higher than that between tetragonal Ce^{3+} and Mn^{2+} ions. Therefore, if Ce^{3+}–Eu^{2+}–Mn^{2+} clusters were formed in the lattice, instead of Ce^{3+}–Eu^{2+} and Ce^{3+}–Mn^{2+} complexes, Mn^{2+} ions would not become sensitized by Ce^{3+} ions since the $Ce^{3+} \rightarrow Eu^{2+}$ energy transfer is much more probable than the $Ce^{3+} \rightarrow Mn^{2+}$ transfer, and this is not in agreement with our experimental observations. This result supports the assumption that energy transfer from tetragonal Ce^{3+}–F_{int}^- ions to Eu^{2+} and Mn^{2+} ions takes place into two different types of clusters (Ce^{3+}–Eu^{2+} and Ce^{3+}–Mn^{2+}). In fact, in accordance with our experimental observation that Eu^{2+} ions do not interact with Mn^{2+} ions, such three-ion clusters would not be formed in the crystalline matrix.

Let us now verify if the critical interaction distance between sensitizer–activator ions results from an ion random distribution or not. Assuming that there is one ion at the centre of a sphere of radius R, then

$$N \frac{4\pi R^3}{3} = 1, \tag{4}$$

where N is the total concentration of sensitizer and activator ions per unit volume. The shorter distance between two randomly distributed ions, D_{random}, can, then, be estimated from the following relationship:

$$D_{random} = 2R = 2\left(\frac{3}{4\pi N}\right)^{1/3}. \tag{5}$$

Thus, the critical Ce^{3+}–Eu^{2+} and Ce^{3+}–Mn^{2+} interaction distances resulted in being smaller than those obtained (~ 95 Å between tetragonal Ce^{3+} and Eu^{2+} ions and ~ 25 Å between tetragonal Ce^{3+} and Mn^{2+} ions) assuming a random ion distribution. It can be inferred, therefore, that the $Ce^{3+} \rightarrow Eu^{2+}$ and $Ce^{3+} \rightarrow Mn^{2+}$ energy transfers arise from small Ce–Eu and Ce–Mn clusters, respectively, instead of from randomly distributed ions.

The ratio of the number of tetragonal Ce^{3+} ions which should be associated with Eu^{2+} or Mn^{2+} ions to the total concentration of tetragonal Ce^{3+}–F_{int}^- ions in the crystal can be estimated

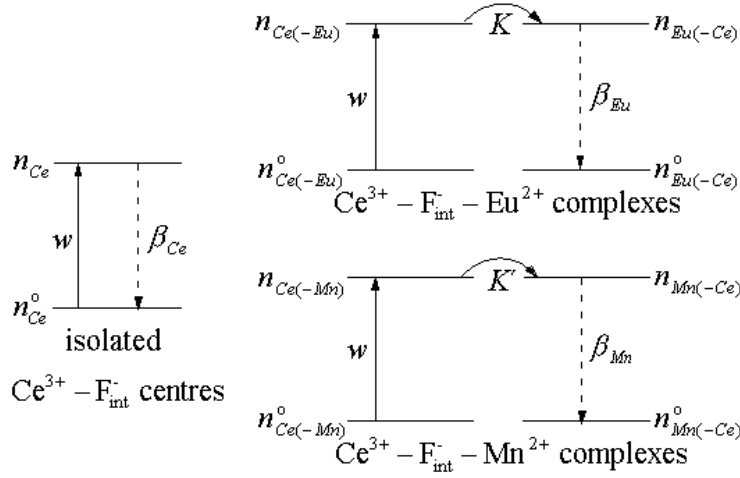**Figure 5.** The energy level system used to describe the kinetics of the Ce^{3+} → Eu^{2+} and Ce^{3+} → Mn^{2+} energy transfers.

using a simple model describing the essential features of the kinetics of the Ce^{3+} → Eu^{2+} and Ce^{3+} → Mn^{2+} energy transfers, in which both the sensitizer (cerium) and activator (europium or manganese) ions are treated as two energy-level systems (figure 5). Taking into account that the calculated energy transfer rates resulted in being quite high compared to the intrinsic radiative decay rate of the tetragonal Ce^{3+} sensitizer ions, it can be assumed that in sensitizer–activator complexes the energy transfer proceeds at a rapid rate that quenches the sensitizer emission completely [12]. This situation means that tetragonal cerium ions clustered with europium or manganese ions do not exhibit any fluorescence. Thus, the observed cerium emission originates exclusively from tetragonal Ce^{3+}–F$_{int}^{-}$ ions, which are not interacting with Eu^{2+} or Mn^{2+} ions. The observed blue and green emissions are due to the Eu^{2+} ion 4f^{6}5d(E$_g$) → 4f^7(^{8}S$_{7/2}$) and Mn^{2+} ion ^{4}T$_{1g}$(G) → ^{6}A$_{1g}$(S) transitions, respectively, which result from excitation by energy transfer from tetragonal cerium ions forming Ce^{3+}–Eu^{2+} and Ce^{3+}–Mn^{2+} impurity clustering.

According to this model, the rate equations describing the time evolution of the excited-state populations of isolated Ce^{3+} ions, and Ce^{3+}–Eu^{2+} and Ce^{3+}–Mn^{2+} complexes are given by:

$$\frac{\mathrm{d}n_{\mathrm{Ce}}}{\mathrm{d}t} = wn_{\mathrm{Ce}}^{\mathrm{o}} - \beta_{\mathrm{Ce}}n_{\mathrm{Ce}},$$

$$\frac{\mathrm{d}n_{\mathrm{Ce(-Eu)}}}{\mathrm{d}t} = wn_{\mathrm{Ce(-Eu)}}^{\mathrm{o}} - Kn_{\mathrm{Ce(-Eu)}},$$

$$\frac{\mathrm{d}n_{\mathrm{Eu(-Ce)}}}{\mathrm{d}t} = Kn_{\mathrm{Ce(-Eu)}} - \beta_{\mathrm{Eu}}n_{\mathrm{Eu(-Ce)}}, \qquad (6)$$

$$\frac{\mathrm{d}n_{\mathrm{Ce(-Mn)}}}{\mathrm{d}t} = wn_{\mathrm{Ce(-Mn)}}^{\mathrm{o}} - K'n_{\mathrm{Ce(-Mn)}},$$

$$\frac{\mathrm{d}n_{\mathrm{Mn(-Ce)}}}{\mathrm{d}t} = K'n_{\mathrm{Ce(-Mn)}} - \beta_{\mathrm{Mn}}n_{\mathrm{Mn(-Ce)}},$$

where n_{Ce} is the concentration of excited state isolated tetragonal Ce^{3+} ions, $n_{\mathrm{Ce(-Eu)}}$ and $n_{\mathrm{Ce(-Mn)}}$ are the concentrations of excited state tetragonal Ce^{3+} ions coupled with excited state Eu^{2+} and Mn^{2+} ions, respectively, $n_{\mathrm{Ce}}^{\mathrm{o}}$, $n_{\mathrm{Ce(-Eu)}}^{\mathrm{o}}$ and $n_{\mathrm{Ce(-Mn)}}^{\mathrm{o}}$ are the corresponding populations

for the ground state, $n_{Eu(-Ce)}$ and $n_{Mn(-Ce)}$ are the concentrations of excited state Eu^{2+} and Mn^{2+} ions coupled with excited state tetragonal Ce^{3+} ions, respectively, w is the absorption probability, which is assumed to be the same for both isolated and coupled tetragonal Ce^{3+} ions, K and K' are the $Ce^{3+} \to Eu^{2+}$ and $Ce^{3+} \to Mn^{2+}$ energy transfer rates, respectively, and β_{Ce}, β_{Eu} and β_{Mn} are the fluorescence decay rates of the isolated tetragonal cerium ions, and europium and manganese ions coupled with tetragonal Ce^{3+}–F_{int}^{-} ions, respectively. The Eu^{2+} and Mn^{2+} activator ion emissions were produced under A-absorption band excitation of tetragonal Ce^{3+}–F_{int}^{-} ions avoiding direct excitation of the activator ions.

Equations (6) can be easily solved for continuous excitation to give the steady-state populations:

$$n_{Ce} = \frac{wn_{Ce}^{o}}{\beta_{Ce}},$$
$$n_{Eu(-Ce)} = \frac{wn_{Ce(-Eu)}^{o}}{\beta_{Eu}}, \tag{7}$$
$$n_{Mn(-Ce)} = \frac{wn_{Ce(-Mn)}^{o}}{\beta_{Mn}}.$$

Considering that the fluorescence intensity of a specific level is equal to the product of the population and the radiative decay rate (β^{r}) of the level, the ratio for the observed emission intensities of coupled Eu^{2+} and isolated tetragonal Ce^{3+} ions (I_{Eu}/I_{Ce}), and that of coupled Mn^{2+} and isolated tetragonal Ce^{3+} ions (I_{Mn}/I_{Ce}), can be expressed as

$$\frac{I_{Eu}}{I_{Ce}} = \frac{n_{Eu(-Ce)}\beta_{Eu}^{r}}{n_{Ce}\beta_{Ce}^{r}}, \tag{8}$$

$$\frac{I_{Mn}}{I_{Ce}} = \frac{n_{Mn(-Ce)}\beta_{Mn}^{r}}{n_{Ce}\beta_{Ce}^{r}}. \tag{9}$$

In the limit of weak pumping, the ground state populations can be considered approximately equal to the corresponding total concentrations: $n_{Ce}^{o} \approx N_{Ce}$, $n_{Ce(-Eu)}^{o} \approx N_{Ce(-Eu)}$ and $n_{Ce(-Mn)}^{o} \approx N_{Ce(-Mn)}$. Thus, from equations (7) to (9) the I_{Eu}/I_{Ce} and I_{Mn}/I_{Ce} rates can be expressed as

$$\frac{I_{Eu}}{I_{Ce}} = \frac{(\beta_{Eu}^{r}/\beta_{Eu})N_{Ce(-Eu)}}{(\beta_{Ce}^{r}/\beta_{Ce})N_{Ce}}, \tag{10}$$

$$\frac{I_{Mn}}{I_{Ce}} = \frac{(\beta_{Mn}^{r}/\beta_{Mn})N_{Ce(-Mn)}}{(\beta_{Ce}^{r}/\beta_{Ce})N_{Ce}}. \tag{11}$$

Finally, the ratio of the number of tetragonal Ce^{3+} ions which should be associated with Eu^{2+} ions $(N_{Ce(-Eu)})$ or Mn^{2+} ions $(N_{Ce(-Mn)})$ to the total concentration of cerium $(N_{T} = N_{Ce} + N_{Ce(-Eu)} + N_{Ce(-Mn)})$ in the crystal can be obtained from equations (10) and (11) after some minor manipulations:

$$\frac{N_{Ce(-Eu)}}{N_{T}} = \frac{1}{(I_{Ce}/I_{Eu})(\beta_{Eu}^{r}/\beta_{Eu})[(\beta_{Ce}/\beta_{Ce}^{r}) + (I_{Mn}/I_{Ce})(\beta_{Mn}/\beta_{Mn}^{r})] + 1}, \tag{12}$$

$$\frac{N_{Ce(-Mn)}}{N_{T}} = \frac{1}{(I_{Ce}/I_{Mn})(\beta_{Mn}^{r}/\beta_{Mn})[(\beta_{Ce}/\beta_{Ce}^{r}) + (I_{Eu}/I_{Ce})(\beta_{Eu}/\beta_{Eu}^{r})] + 1}. \tag{13}$$

Using $\beta_{Mn} \approx 2\beta_{Mn}^{r}$, $\beta_{Ce}^{r} \approx \beta_{Ce}$ [20] and $\beta_{Eu}^{r} \approx \beta_{Eu}$ [13], $N_{Ce(-Eu)}/N_{T}$ and $N_{Ce(-Mn)}/N_{T}$ resulted in being about 4×10^{-4} and 0.23, respectively, when our experimentally determined ratios for $I_{Eu}/I_{Ce} = 5 \times 10^{-4}$ and $I_{Mn}/I_{Ce} = 0.15$ are used in equations (12) and (13). Therefore, about 0.04% and 23% of the total concentration of tetragonal Ce^{3+} ions appear to

be associated with Eu^{2+} and Mn^{2+} ions, respectively. Otherwise, in relation to the estimated total concentration of activator ions, $\sim$9% of Eu^{2+} ions and $\sim$0.4% of Mn^{2+} ions interact with tetragonal Ce^{3+} ions.

5. Conclusions

The spectroscopic data obtained in calcium fluoride doped with $\sim$165 ppm of Ce^{3+} ions, $\sim$3446 ppm of Mn^{2+} ions, and unintentionally doped with Eu^{2+} ions ($<$1 ppm), indicate that Ce$^{3+} \rightarrow$ Eu^{2+} and Ce$^{3+} \rightarrow$ Mn^{2+} energy transfer processes taking place in this material occur as a consequence of these ions to form small Ce^{3+}–Eu^{2+} and Ce^{3+}–Mn^{2+} clusters. In fact, our experimental data can only be explained assuming that an electric dipole–dipole interaction mechanism occurs in the Ce^{3+}–Eu^{2+} clusters and an electric dipole–quadrupole one occurs in the Ce^{3+}–Mn^{2+} clusters. Our spectroscopic data also revealed that Mn^{2+} ions do not become sensitized by Eu^{2+} ions, in contrast to the energy transfer from Eu^{2+} to Mn^{2+} ions observed in CaF$_2$ doubly doped with these ions. This finding might suggest that Eu^{2+} ions prefer to cluster with tetragonal Ce^{3+} ions, when these ions are also present in the crystal. Such a preferential impurity clustering, which has been considered to be infrequent in most studies of energy transfer between impurities in solids, appears to be a quite relevant finding for the design of more efficient laser systems as well as more efficient conversion phosphors of light UV (Ce^{3+} ion absorption) to blue (Eu^{2+} ion emission) and green (Mn^{2+} ion emission).

Acknowledgments

References

[1] Lahoz F, Daran E, Lifante G, Balaji T and Munoz-Yague A 1999 *Appl. Phys. Lett.* **74** 1060
[2] Golding P S, Jackson S D, King T A and Pollnau M 2000 *Phys. Rev.* B **62** 856
[3] Strohhofer C, Kik P G and Polman A 2000 *J. Appl. Phys.* **88** 4486
[4] Park S H, Lee D C, Heo J and Shin D W 2002 *J. Appl. Phys.* **91** 9072
[5] Jia D, Meltzer R S, Yen W M, Jia W and Wang X 2002 *Appl. Phys. Lett.* **80** 1535
[6] Bosze E J, Hirata G A, Shea-Rohwer L E and McKittrick J 2003 *J. Lumin.* **104** 47
[7] Braud A, Girard S, Doualan J L, Thuau M, Moncorge R and Tkachuk A M 2000 *Phys. Rev.* B **61** 5280
[8] Vega-Duran J T, Diaz-Torres L A, Meneses-Nava M A, Maldonado-Rivera J L and Barbosa-Garcia O 2001 *J. Phys. D: Appl. Phys.* **34** 3203
[9] Dorenbos P and den Hartog H W 1985 *Phys. Rev.* B **31** 3939
[10] McKeever S W S, Jassemnejad B, Brown M D, Mathur V K, Abbundi R J and Chan H 1986 *Radiat. Eff.* **99** 15
[11] McKeever S W S, Brown M D, Abbundi R J, Chan H and Mathur V K 1986 *J. Appl. Phys.* **60** 2505
[12] Caldiño U G 2003 *J. Phys.: Condens. Matter* **15** 3821
[13] Caldiño U G, Muñoz A F and Rubio J O 1990 *J. Phys.: Condens. Matter* **2** 6071
[14] Caldiño U G, de la Cruz C, Muñoz G H and Rubio J O 1989 *Solid State Commun.* **69** 347
[15] Denks V P, Kerikmyae M P, Lust A L and Savikhina T I 2000 *Phys. Solid State* **42** 261
[16] Lira A, Dagdug L, Méndez A, Murrieta H and Caldiño U G 1999 *Phys. Status Solidi* b **212** 199
[17] McKeever S W S, Jassemnejad B, Landreth J F and Brown M D 1986 *J. Appl. Phys.* **60** 1124
[18] Loh E 1968 *Phys. Rev.* **175** 533
[19] Kobayasi T, Mroczkowski S, Owen J F and Brixner L H 1980 *J. Lumin.* **21** 247
[20] Bril A, Klasns H A and Zalm P 1953 *Philips Res. Rep.* **8** 393
[21] Alonso P J and Alcalá R 1981 *J. Lumin.* **22** 321
[22] Jeon H S, Kim S K, Kim T W, Chang S K, Jeong K, Choi J C and Park H L 2000 *MRS Bull.* **35** 1447
[23] Lin H, Liu X R and Pun E Y B 2002 *Opt. Mater.* **18** 397
[24] Dexter D L 1953 *J. Chem. Phys.* **21** 836
[25] Blasse G 1969 *Philips Res. Rep.* **24** 131